

Construction of ZnCo₂O₄/Ag₃PO₄ composite photocatalyst for enhanced photocatalytic performance

Jiafeng Hu¹, Jiayi Liu², Hao Hu¹, Xiaotao Zhou¹, Qiwei Wang³, Weizhi Wei³, and Wenhui Liu²

¹Chinese People's Liberation Army

²North University of China

³Army Engineering University of PLA

June 19, 2023

Abstract

In this study, a ZnCo₂O₄/Ag₃PO₄ composite catalyst was prepared by the precipitation method, and its photocatalytic degradation activity for methyl orange (MO) was studied. The catalysts were characterized by TEM, XRD, EDX, HRTEM, SAED, SEM, XPS, and UV-Vis-DRS. The results indicate that 0.1 ZnCo₂O₄/Ag₃PO₄ The composite system has a good photocatalytic degradation effect on methyl orange. Under 30-minute simulated sunlight conditions, the degradation rate can reach 94%. The results show that the maximum reaction rate constant of 0.1 ZnCo₂O₄/Ag₃PO₄ is 0.05301 min⁻¹, which is three times the size of pure Ag₃PO₄ and 52 times the size of pure ZnCo₂O₄. After three cycles, 0.1 ZnCo₂O₄/Ag₃PO₄ still degraded methyl orange (MO) at a rate of 84.4%. The trapping experiment showed that hole (h⁺) and O₂⁻ played the most important roles in the photocatalytic degradation field of methyl orange (MO) by 0.1 ZnCo₂O₄/Ag₃PO₄, and hydroxyl radical (OH[·]) played a partial role. The energy level structure of ZnCo₂O₄/Ag₃PO₄ is conducive to the effective separation of photogenerated electrons and holes, improving the lifespan of photogenerated charges. Among them, the photocatalytic performance of 0.1 ZnCo₂O₄/Ag₃PO₄ is the most excellent.

Title page

Construction of ZnCo₂O₄/Ag₃PO₄ composite photocatalyst for enhanced photocatalytic performance

Jiafeng Hu^{a,b}, Jiayi Liu^{c*}, Hao Hu^a, Xiaotao Zhou^a, Qiwei Wang^b, Weizhi, Wei^b, Wenhui Liu^{c*}

Jiafeng Hu was responsible for conducting the experiment and writing the article. Jiayi Liu and Wenhui Liu was mainly responsible for guiding the experiment and the writing of the article. Hao Hu, Xiaotao Zhou, Qiwei Wang, and Weizhi, Wei participated in some of the experiments and data analysis.

^a 75714 troops of the Chinese people's liberation army, Hengyang, 421000, PR China

^b Army Engineering University of PLA, Nanjing 210007, PR China.

^c Environmental and Safety Engineering Institute, North University of China, Taiyuan, Shanxi 030051, People's Republic of China

E-mail: H892601280@163.com (Jiafeng Hu), 827487598@qq.com (Jiayi Liu),

HUhao75714@163.com (Hao Hu), ZHOUxiaotao778812@163.com (Xiaotao Zhou), wangqiwei_83@126.com (Qiwei Wang) and weiweizhi0517@163.com (Weizhi Wei)

Corresponding Author

* Jiayi Liu, E-mail: 827487598@qq.com and *Wenhui Liu, E-mail: wenhuiliuzb@163.com

Funding: None

Conflict of interest statement: The authors declared that they have no conflicts of interest to this work. We declare that we do not have any commercial or associative interest that represents a conflict of interest in connection with the work submitted.

Permission to reproduce materials from other sources: None

Data Availability statement: The data used to support the findings of this study are available from the corresponding author upon request.

Abstract: In this study, a $\text{ZnCo}_2\text{O}_4/\text{Ag}_3\text{PO}_4$ composite catalyst was prepared by the precipitation method, and its photocatalytic degradation activity for methyl orange (MO) was studied. The catalysts were characterized by TEM, XRD, EDX, HRTEM, SAED, SEM, XPS, and UV-Vis-DRS. The results indicate that 0.1 $\text{ZnCo}_2\text{O}_4/\text{Ag}_3\text{PO}_4$ The composite system has a good photocatalytic degradation effect on methyl orange. Under 30-minute simulated sunlight conditions, the degradation rate can reach 94%. The results show that the maximum reaction rate constant of 0.1 $\text{ZnCo}_2\text{O}_4/\text{Ag}_3\text{PO}_4$ is 0.05301 min^{-1} , which is three times the size of pure Ag_3PO_4 and 52 times the size of pure ZnCo_2O_4 . After three cycles, 0.1 $\text{ZnCo}_2\text{O}_4/\text{Ag}_3\text{PO}_4$ still degraded methyl orange (MO) at a rate of 84.4%. The trapping experiment showed that hole (h^+) and O_2^- played the most important roles in the photocatalytic degradation field of methyl orange (MO) by 0.1 $\text{ZnCo}_2\text{O}_4/\text{Ag}_3\text{PO}_4$, and hydroxyl radical ($\text{OH}\cdot$) played a partial role. The energy level structure of $\text{ZnCo}_2\text{O}_4/\text{Ag}_3\text{PO}_4$ is conducive to the effective separation of photogenerated electrons and holes, improving the lifespan of photogenerated charges. Among them, the photocatalytic performance of 0.1 $\text{ZnCo}_2\text{O}_4/\text{Ag}_3\text{PO}_4$ is the most excellent.

Keywords: methyl orange; photocatalytic activity; photogenerated carriers

1. Introduction

At present, the form of global environmental pollution is severe, and environmental problems pose a major threat to mankind [1-3]. Solar energy is a renewable energy source, but its development is greatly limited due to its low utilization rate and severe environmental pollution. Therefore, how to efficiently use solar energy and effectively manage environmental pollution has become an important issue that human society is facing and urgently needs to solve [4-5]. Semiconductor photocatalytic technology provides a new choice for solving the problem of global environmental pollution [6-7]. Since TiO_2 was first used as a photoanode to decompose water under UV irradiation in the 1970s [8], the application of nano- TiO_2 semiconductor photocatalytic oxidation technology in the field of environmental pollution control has opened a new chapter. The so-called photocatalytic reaction is a process in which the reaction system containing the catalyst excites reaction molecules under light irradiation or excites the catalyst to form complexes with reaction molecules to transform light power into chemical power and improve reaction efficiency [9]. However, due to the large band gap of TiO_2 , its photocatalytic reaction can only be carried out under ultraviolet light, and the utilization rate of sunlight is low. In response to this practical issue, people have been committed to developing efficient visible-light catalytic materials. In response to this issue, this project aims to further optimize the photocatalytic performance of TiO_2 based on preliminary work. At present, the main research methods include precious metal deposition, co-doping, metal ion doping, etc. At the same time, they are also researching new photocatalytic materials.

Ag_3PO_4 has high photocatalytic efficiency and can degrade organic pollutants under the conditions of sunlight and visible light. However, Ag_3PO_4 is easily reduced to elemental Ag under visible light irradiation [10], which restricts its practical use. In order to better utilize sunlight as a clean energy source, people have conducted extensive research and development. Therefore, people organically combine these two types of semiconductors with different band structures, hoping to accelerate the separation of photogenerated charge carriers and enhance their photocatalytic activity.

Zhang et al. prepared an $\text{Ag}_3\text{PO}_4/\text{SnO}_2$ composite photocatalyst by combining Ag_3PO_4 and SnO_2 , which not

only showed strong photocatalytic performance but also enhanced the stability of the composite [11]. In the experiment of degrading methyl orange wastewater, the reusability and stability of $\text{Ag}_3\text{PO}_4/\text{TiO}_2$ composite photocatalytic material prepared by Li et al. were significantly improved compared with Ag_3PO_4 and TiO_2 [12]. Liu et al. synthesized $\text{Bi}_2\text{GeO}_5/\text{Ag}_3\text{PO}_4$ nanocomposites by a two-step method and formed Z-type heterojunctions through a subsequent photocatalytic process, which significantly improved their photocatalytic activity and stability [13].

In this paper, ZnCo_2O_4 nanoparticles were prepared by microwave assisted method and then deposited on Ag_3PO_4 surface by precipitation method to form $\text{ZnCo}_2\text{O}_4/\text{Ag}_3\text{PO}_4$ composite catalyst. The structure of the composite was characterized, and its degradation performance in methyl orange wastewater was studied under visible light. Results indicate that ZnCo_2O_4 can availably improve the stability and photocatalytic degradation properties of Ag_3PO_4 .

2. Experimental section

2.1. Experiment reagents

The reagents used in the experiment are shown in Table 1.

Table 1 Experiment reagents

Medications designation	Chemical formula	Purity	Manufacturer
Zinc nitrate	$\text{Zn}(\text{NO}_3)_2 \cdot 6\text{H}_2\text{O}$	AR	Sinopharm Chemical Reagent Co
Cobaltous nitrate hexahydrate	$\text{Co}(\text{NO}_3)_3 \cdot 6\text{H}_2\text{O}$	AR	Sinopharm Chemical Reagent Co
Urea	$\text{CO}(\text{NH}_2)_2$	AR	Sinopharm Chemical Reagent Co
Ammonium fluoride	NH_4F	AR	Sinopharm Chemical Reagent Co
Silver nitrate	AgNO_3	AR	Sinopharm Chemical Reagent Co
Disodium hydrogen phosphate	$\text{Na}_2\text{HPO}_4 \cdot 12\text{H}_2\text{O}$	AR	Sinopharm Chemical Reagent Co
1,4-Benzoquinone	$\text{C}_6\text{H}_4\text{O}_2$	AR	Sinopharm Chemical Reagent Co
Triethanolamine	$\text{N}(\text{CH}_2\text{CH}_2\text{OH})_3$	AR	Sinopharm Chemical Reagent Co
Isopropanol	$(\text{CH}_3)_2\text{CHOH}$	AR	Sinopharm Chemical Reagent Co
Ethanol	$\text{CH}_2\text{CH}_3\text{OH}$	AR	Sinopharm Chemical Reagent Co
Methyl orange	$\text{C}_{14}\text{H}_{14}\text{N}_3\text{SO}_3\text{S}$	AR	Sinopharm Chemical Reagent Co

2.2. Characterization instruments

The characterization instruments and test conditions used in the experiment are shown in Table 2.

Table 2 Characterization instruments

Characterization instruments	Version	Test Conditions
Scanning electron microscope (SEM)	JSM-6510	/
High resolution transmission electron microscope (HRTEM)	JEM-2100	/
X-ray diffraction (XRD)	Rigaku D/max-2500	X-ray diffractometer at 35 kV, ranging
X-ray photoelectron spectroscopy (XPS)	ESCALAB 250	/
UV-visible diffuse reflectance spectra (DRS)	UV-2550	wavelength between 200 and 850nm

2.3. Preparation of catalyst

2.3.1. Synthesis of the ZnCo_2O_4

A microwave-assisted synthesis method was used to synthesize ZnCo_2O_4 particles. The specific preparation process is as follows: 7.5 mmol of $\text{Zn}(\text{NO}_3)_2 \cdot 6\text{H}_2\text{O}$, 15 mmol of $\text{Co}(\text{NO}_3)_3 \cdot 6\text{H}_2\text{O}$, 60 mmol of $\text{CO}(\text{NH}_2)_2$ and

12 mmol of NH_4F were successively added to 100 ml of deionized water, using a magnetic stirrer to stir for 30 minutes and ultrasound for 30 minutes to completely dissolve the medicine and form a light pink solution. Then transfer the mixed solution to a 300 ml polytetrafluoroethylene reaction tank, assemble the reaction instrument, and place it in the microwave device, heating at a rate of $8\text{ }^\circ\text{C}/\text{min}$ and microwave reaction at $130\text{ }^\circ\text{C}$ for 30 min. When the reaction is complete, the product temperature is brought to room temperature, and then the drug is collected by centrifugation, filtration, and repeat washing with deionized water, dried in the oven at $80\text{ }^\circ\text{C}$ for 10 hours, and finally calcined in the tubular muffle furnace at $350\text{ }^\circ\text{C}$ for 2 hours at a heating rate of $1\text{ }^\circ\text{C}/\text{min}$ to obtain the product, which is collected for standby.

2.3.2. Preparation of the $\text{ZnCo}_2\text{O}_4/\text{Ag}_3\text{PO}_4$ Composites

0.612g AgNO_3 was added to 30 ml of silver nitrate solution, and also ZnCo_2O_4 (0.1g, 0.2 g, and 0.3g) was added to the silver nitrate solution, sonicated for 30 min to disperse ZnCo_2O_4 evenly, then slowly added to 30 ml of solution having 0.43g $\text{Na}_2\text{HPO}_4 \cdot 12\text{H}_2\text{O}$ and stirred at room temperature for 120 min. After that, the product was filtered and precipitated by centrifugation, cleaned with deionized water and anhydrous ethanol, dried at $60\text{ }^\circ\text{C}$, and three $\text{ZnCo}_2\text{O}_4/\text{Ag}_3\text{PO}_4$ catalysts with different ZnCo_2O_4 contents were obtained, which were labeled as 0.1 $\text{ZnCo}_2\text{O}_4/\text{Ag}_3\text{PO}_4$, 0.2 $\text{ZnCo}_2\text{O}_4/\text{Ag}_3\text{PO}_4$, and 0.3 $\text{ZnCo}_2\text{O}_4/\text{Ag}_3\text{PO}_4$, respectively. A single Ag_3PO_4 was prepared for comparative study.

2.4. Photocatalytic experiment

The photocatalytic experiment was carried out in a photochemical reactor. A xenon lamp (1000 W) simulates sunlight. Weigh 50 mg of photocatalyst, scatter it into a beaker with 50 ml of 10 mg/L methyl orange, put it in the photochemical reactor, close the box door to avoid alternating light and dark, stir and adsorb for 20 minutes, turn on the light source, take 4 ml of samples every 5 minutes, and take the supernatant after centrifugation. The absorbance of the methyl orange solution before and after the reaction was measured by a UV-Vis spectrophotometer at 464 nm. During the reaction, hold the reaction suspension at about $10\text{ }^\circ\text{C}$. Beer Lambert's Law was used to calculate the degradation rate of photocatalytic degradation of MO. Characterization of photocatalytic degradation of MO using the kinetic equation method:

$$\frac{C_t}{C_0} = \frac{A_t}{A_0} \quad (1)$$

$$A_t + Kt = -\ln\left(\frac{C_t}{C_0}\right) \quad (2)$$

A_0 and A_t show the absorbance of the solution at the initial and post-irradiation times, and C_0 and C_t show the corresponding initial concentration of the solution and the solution concentration after t time.

Catalyst cycle stability analysis: collect the photocatalyst after each use, wash and dry it many times, and repeat the above steps twice to investigate its cycle stability.

Free radical capture experiment: Using isopropanol (IPA) as hydroxyl radical ($\text{OH}\cdot$) trapping agent, triethanolamine (TEOA) as hole (h^+) trapping agent, and p-benzoquinone (BQ) as superoxide radical ($\text{O}_2\cdot^-$) trapping agent, the active factors in the catalytic degradation process of the objective contaminant were analyzed through the change in degradation efficiency before and after the addition of trapping agent.

3. Results and Discussion

3.1. Catalyst characterization

Figure 1 The XRD optical spectrum of Ag_3PO_4 , ZnCo_2O_4 , 0.1 $\text{ZnCo}_2\text{O}_4/\text{Ag}_3\text{PO}_4$, 0.2 $\text{ZnCo}_2\text{O}_4/\text{Ag}_3\text{PO}_4$ and 0.3 $\text{ZnCo}_2\text{O}_4/\text{Ag}_3\text{PO}_4$.

The XRD spectra of the prepared Ag_3PO_4 , ZnCo_2O_4 , 0.1 $\text{ZnCo}_2\text{O}_4/\text{Ag}_3\text{PO}_4$, 0.2 $\text{ZnCo}_2\text{O}_4/\text{Ag}_3\text{PO}_4$, and 0.3 $\text{ZnCo}_2\text{O}_4/\text{Ag}_3\text{PO}_4$ catalysts are shown in Fig. 1. It can be seen from the figure that the diffraction peaks located at 18.96° , 31.22° , 36.81° , 44.74° , 59.28° , and 65.15° in the XRD pattern of ZnCo_2O_4 (JCPDS No. 23-1390) belong to the (111), (220), (210), (311), (400), (511), and (440) crystal planes, indicating that ZnCo_2O_4 was synthesized by the microwave-assisted method. The characteristic diffraction peaks located at 20.9° , 29.7° , 33.3° , 36.6° , 47.9° , 52.8° , 55.1° , 57.4° , 61.7° , and 72.0° in the XRD spectrum of Ag_3PO_4 catalyst correspond to

the (110), (200), (210), (211), (310), (222), (320), (321), (400), and (421) crystallographic planes of Ag_3PO_4 , which are consistent with the standard card of Ag_3PO_4 (JCPDS No. 70-0702). The characteristic diffraction peaks belonging to ZnCo_2O_4 in the XRD pattern of $\text{ZnCo}_2\text{O}_4/\text{Ag}_3\text{PO}_4$ became more and more obvious with the increase in the amount of ZnCo_2O_4 , which indicated that the ZnCo_2O_4 particles were successfully loaded onto the surface of Ag_3PO_4 to form the $\text{ZnCo}_2\text{O}_4/\text{Ag}_3\text{PO}_4$ composite catalyst.

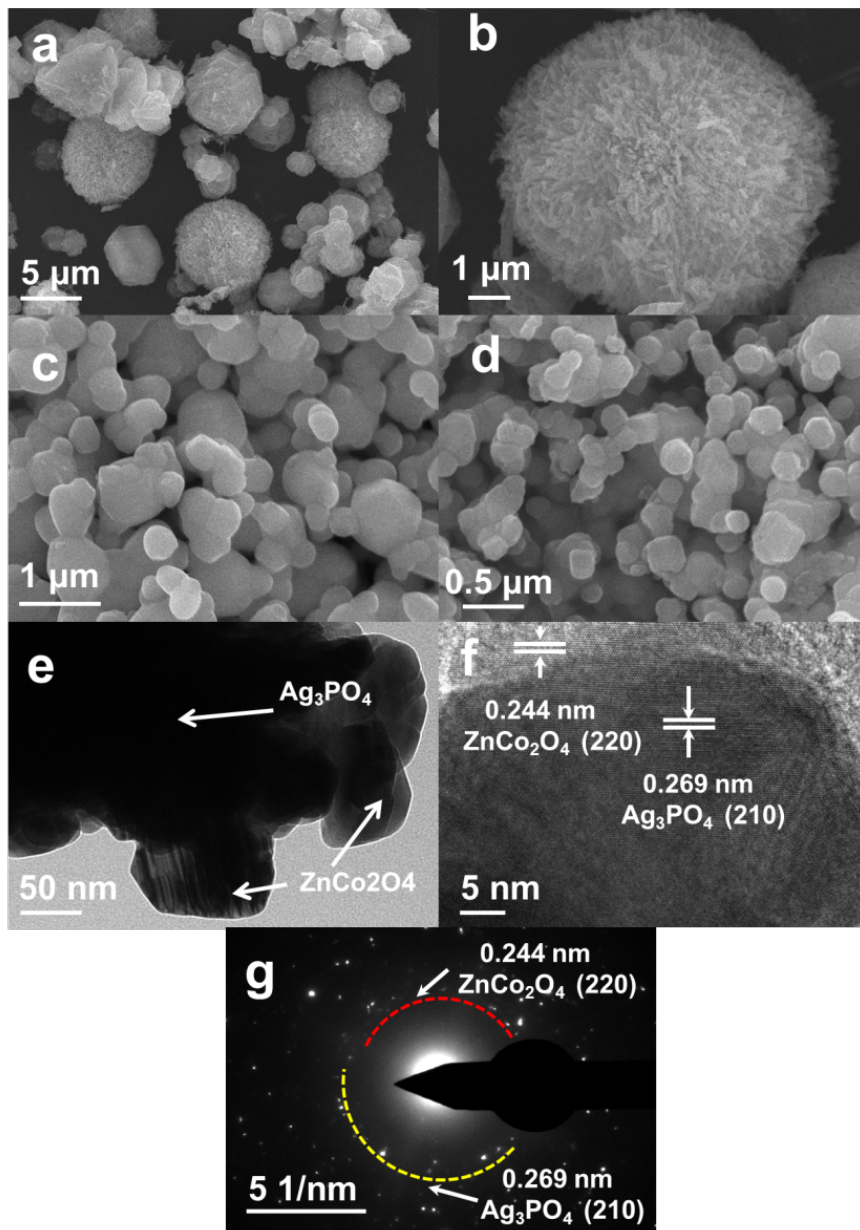


Figure 2 a Low and b high-magnification SEM images of ZnCo_2O_4 ; c SEM images of Ag_3PO_4 ; d SEM images of $\text{ZnCo}_2\text{O}_4/\text{Ag}_3\text{PO}_4$; e TEM image of $\text{ZnCo}_2\text{O}_4/\text{Ag}_3\text{PO}_4$; f HRTEM image of $\text{ZnCo}_2\text{O}_4/\text{Ag}_3\text{PO}_4$ and g SAED pattern of $\text{ZnCo}_2\text{O}_4/\text{Ag}_3\text{PO}_4$.

Fig. 2a shows the spherical ZnCo_2O_4 successfully synthesized by the microwave-assisted method with a

diameter range of 3–8 μm . Fig. 2b shows the structure of a single ZnCo_2O_4 microsphere, which can be seen from the figure as a stack of nanosheets. Fig. 2c shows Ag_3PO_4 crystals with a regular hexahedral structure and a particle size range of 0.4–1 μm . Fig. 2d is an SEM image of the composite $\text{ZnCo}_2\text{O}_4/\text{Ag}_3\text{PO}_4$. It can be seen from the figure that the particle size range of $\text{ZnCo}_2\text{O}_4/\text{Ag}_3\text{PO}_4$ is also 0.4–1 μm , which is caused by the recrystallization of ZnCo_2O_4 and deposition on Ag_3PO_4 during the synthesis process. To further observe the morphology of $\text{ZnCo}_2\text{O}_4/\text{Ag}_3\text{PO}_4$, Fig. 2e shows the TEM image of $\text{ZnCo}_2\text{O}_4/\text{Ag}_3\text{PO}_4$, from which it can be seen that the recrystallized ZnCo_2O_4 is attached to the Ag_3PO_4 crystal surface. Fig. 2f shows the HRTEM image of $\text{ZnCo}_2\text{O}_4/\text{Ag}_3\text{PO}_4$, which further verifies that the recrystallized ZnCo_2O_4 is successfully attached to the Ag_3PO_4 crystal surface, and the lattice spacing d is 0.244 and 0.269 nm for ZnCo_2O_4 and Ag_3PO_4 , corresponding to the (220) and (210) crystal planes of ZnCo_2O_4 and Ag_3PO_4 , respectively. Fig. 2g shows the SAED plot of $\text{ZnCo}_2\text{O}_4/\text{Ag}_3\text{PO}_4$, in which the bright diffraction rings of $\text{ZnCo}_2\text{O}_4/\text{Ag}_3\text{PO}_4$ can be seen, indicating that it is polycrystalline. In addition, the lattice distances of 0.244 nm and 0.269 nm for the two crystal planes can be clearly seen in Fig. 2g, which is in agreement with the results of HRTEM plots. In summary, it can be clearly seen that the composite catalyst $\text{ZnCo}_2\text{O}_4/\text{Ag}_3\text{PO}_4$ is formed by loading the recrystallized ZnCo_2O_4 onto the Ag_3PO_4 crystal surface.

Hosted file

image3.wmf available at <https://authorea.com/users/630614/articles/650303-construction-of-znco2o4-ag3po4-composite-photocatalyst-for-enhanced-photocatalytic-performance>

Figure 3 XPS spectra of $\text{ZnCo}_2\text{O}_4/\text{Ag}_3\text{PO}_4$: (a) survey scan, (b) Ag 3d, (c) O 1s, (d) Zn 2p, (e) P 2p, (f) Co 2p.

The XPS of $\text{ZnCo}_2\text{O}_4/\text{Ag}_3\text{PO}_4$ is shown in Fig. 3. Fig. 3a shows the full spectrum scan of $\text{ZnCo}_2\text{O}_4/\text{Ag}_3\text{PO}_4$, from which it can be seen that the product has six elementary substances: Ag, O, Zn, C, P, and Co, where C is the substrate. Fig. 3b shows the XPS spectrum peaks of Ag 3d. The peaks at 367.85 eV and 373.8 eV in Ag 3d correspond to Ag 3d_{5/2} and Ag 3d_{3/2}, respectively. Ag 3d_{5/2} can be decomposed into two peaks at 367.75 eV and 368.20 eV, while Ag 3d_{3/2} can also be decomposed into two peaks at 373.8 eV and 374.4 eV. The peaks appearing at 367.75 eV and 373.8 eV belong to Ag⁺, while the peaks at 368.2 eV and 374.4 eV belong to Ag⁰ monomer, which indicates that the Ag in the catalyst exists mainly in the form of Ag⁺ [13, 14]. Fig. 3c shows the XPS spectrum of O 1s. The whole peak can be split into three feature peaks: 530.35 eV, 530.8 eV, and 532.2 eV. Among the three characteristic peaks, 530.35 eV and 530.8 eV corresponded to Ag_3PO_4 and ZnCo_2O_4 lattices in the material, respectively. The peak at 532.2 eV manifests H₂O or OH⁻ adsorbed on the material surface [15]. Fig. 3d is the XPS analytical diagram of Zn 2p. There are two main peaks at 1021.6 eV and 1044.7 eV, corresponding to the regional of Zn 2p_{3/2} and Zn 2p_{1/2} [16, 17]. It can be seen that the peak of Zn 2p_{3/2} is a single peak near 1021.6 eV, which is typical of the oxidation state of Zn²⁺. Fig. 3e indicates the XPS peak of P 2p, corresponding to P⁵⁺ in PO₃+ 4 structure at 132.45 eV. Fig. 3f is the XPS analytical diagram of Co 2p. There are two main peaks at 780.8 eV and 795.9 eV, corresponding to the regional of Co 2p_{1/2} and Co 2p_{3/2}, and the obvious satellite peaks observed at 780.8 eV are characteristic peaks of the Co³⁺ oxidation state [18, 19]. XPS analysis further proved that ZnCo_2O_4 and Ag_3PO_4 were compounded.

Figure 4 a UV-Vis DRS results of Ag_3PO_4 , ZnCo_2O_4 and 0.1 $\text{ZnCo}_2\text{O}_4/\text{Ag}_3\text{PO}_4$; **b** Plots of $(\alpha hv)^2$ as a function of energy (hv) for bandgap energies of Ag_3PO_4 , ZnCo_2O_4 and 0.1 $\text{ZnCo}_2\text{O}_4/\text{Ag}_3\text{PO}_4$.

Fig. 4a shows the UV-Vis diffuse absorption spectra of Ag_3PO_4 , ZnCo_2O_4 , and 0.1 $\text{ZnCo}_2\text{O}_4/\text{Ag}_3\text{PO}_4$ catalysts. The light absorption intensity of ZnCo_2O_4 is stronger in the whole wavelength range, while Ag_3PO_4 absorbs wider in the visible light region with an absorption boundary of approximately 530 nm. The addition of ZnCo_2O_4 widens the Ag_3PO_4 light absorption range and also raises the light absorption intensity, which indicates that ZnCo_2O_4 has a synergistic effect with Ag_3PO_4 .

According to the Kubelka-Munk formula, the band gap width of Ag_3PO_4 and ZnCo_2O_4 can be counted [20]:

$$\alpha hv = A (hv - E_g)^{\frac{n}{2}} \quad (3)$$

In this equation, α and h are the absorption coefficient and Planck constant, E_g is the energy band gap, V is the optical frequency, and a is the constant. n represents the optical transition type of the semiconductor. When the semiconductor has a direct band gap, n is 1, and when the semiconductor has an indirect band gap, n is 4. Since ZnCo_2O_4 and Ag_3PO_4 are direct semiconductors, n is taken as 1 [19, 21]. Fig. 4b shows the $(\alpha h\nu)^2$ versus energy ($h\nu$) of band gap energy for Ag_3PO_4 , ZnCo_2O_4 , and 0.1 $\text{ZnCo}_2\text{O}_4/\text{Ag}_3\text{PO}_4$ catalysts, in which the band gap widths of ZnCo_2O_4 and Ag_3PO_4 are 2.63 eV and 2.45 eV, respectively.

In order to show the carrier transfer of $\text{ZnCo}_2\text{O}_4/\text{Ag}_3\text{PO}_4$ catalyst in the process of photocatalytic reaction, the VB and CB potentials of ZnCo_2O_4 and Ag_3PO_4 were forecasted by this formula [22]:

$$E_{\text{CB}} = X - E_e - 0.5E_g \quad (4)$$

$$E_{\text{VB}} = E_{\text{CB}} + E_g \quad (5)$$

Where x is the absolute electronegativity of the semiconductor, E_e is the potential of the free electron relative to the standard hydrogen electrode (about 4.5 eV), E_g is the band gap width of the semiconductor, and E_{CB} and E_{VB} are the conduction band and valence band potentials of semiconductors, respectively. X values of ZnCo_2O_4 and Ag_3PO_4 are 5.96 eV and 6.17 eV, and the E_{VB} values of ZnCo_2O_4 and Ag_3PO_4 can be calculated to be 2.775 eV and 2.9 eV, respectively. Therefore, the E_{CB} values of ZnCo_2O_4 and Ag_3PO_4 are estimated to be 0.145 eV and 0.45 eV, respectively.

3.2. Photocatalytic properties and mechanism

Figure 5 a Visible light scanning pattern of MO degradation by 0.1 $\text{ZnCo}_2\text{O}_4/\text{Ag}_3\text{PO}_4$; b Effects of different catalysts on photocatalytic degradation of MO under visible light; c First-order kinetic fitting plots of MO degradation by each catalysts; d Cycling runs of Ag_3PO_4 and 0.1 $\text{ZnCo}_2\text{O}_4/\text{Ag}_3\text{PO}_4$ for the degradation of MO.

Table 3 Photodegradation rate constants and linear regression coefficients of different catalysts obtained according to the formula: $-\ln(C/C_0) = kt$.

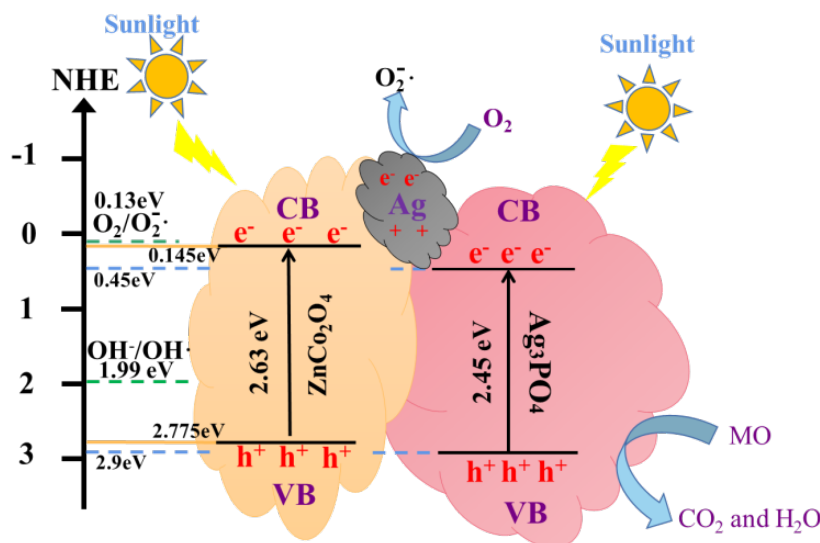
	K(min ⁻¹)	Regression equation	R ²
0.1 $\text{ZnCo}_2\text{O}_4/\text{Ag}_3\text{PO}_4$	0.05301	$-\ln(C/C_0)=0.05301x+0.34031$	R ² =0.70906
0.2 $\text{ZnCo}_2\text{O}_4/\text{Ag}_3\text{PO}_4$	0.0229	$-\ln(C/C_0)=0.0229x+0.18005$	R ² =0.77862
0.3 $\text{ZnCo}_2\text{O}_4/\text{Ag}_3\text{PO}_4$	0.02006	$-\ln(C/C_0)=0.02006x+0.15152$	R ² =0.76032
Ag_3PO_4	0.01793	$-\ln(C/C_0)=0.01793x+0.16102$	R ² =0.83218
ZnCo_2O_4	0.00102	$-\ln(C/C_0)=0.00102x+0.02698$	R ² =0.92847

In Figure 5a, the photocatalytic degradation of 0.1 $\text{ZnCo}_2\text{O}_4/\text{Ag}_3\text{PO}_4$ was analyzed using UV-vis full wave scanning of methyl orange molecules. The results showed that the characteristic peak intensity of methyl orange molecules decreased with the prolongation of reaction time near 464nm, and after 30 minutes, its peak intensity approached 0, indicating that methyl orange had been completely degraded. Fig. 5b shows the photocatalytic degradation of MO by different catalysts Ag_3PO_4 , ZnCo_2O_4 , 0.1 $\text{ZnCo}_2\text{O}_4/\text{Ag}_3\text{PO}_4$, 0.2 $\text{ZnCo}_2\text{O}_4/\text{Ag}_3\text{PO}_4$, and 0.3 $\text{ZnCo}_2\text{O}_4/\text{Ag}_3\text{PO}_4$. The results showed that the photocatalytic effect of pure ZnCo_2O_4 was the worst, and the photocatalytic degradation rate was only 5% within 30 min. While Ag_3PO_4 , 0.2 $\text{ZnCo}_2\text{O}_4/\text{Ag}_3\text{PO}_4$, and 0.3 $\text{ZnCo}_2\text{O}_4/\text{Ag}_3\text{PO}_4$ showed 56%, 69%, and 65% photocatalytic degradation at 30 min, respectively. The results showed that the 0.1 $\text{ZnCo}_2\text{O}_4/\text{Ag}_3\text{PO}_4$ catalyst had the best photocatalytic degradation effect on methyl orange, and after 30 minutes, the degradation rate of methyl orange could reach 94%. This study found that ZnCo_2O_4 can effectively improve the photocatalytic degradation performance of Ag_3PO_4 . Fig. 5c shows that the reaction of $\text{ZnCo}_2\text{O}_4/\text{Ag}_3\text{PO}_4$ photocatalytic degradation of methyl orange follows the pseudo first-order reaction kinetic model. As shown in Table 3, calculate the k-value of each sample after linearly fitting the curve, and the reaction rate constants of Ag_3PO_4 , ZnCo_2O_4 , 0.1 $\text{ZnCo}_2\text{O}_4/\text{Ag}_3\text{PO}_4$, 0.2 $\text{ZnCo}_2\text{O}_4/\text{Ag}_3\text{PO}_4$, and 0.3 $\text{ZnCo}_2\text{O}_4/\text{Ag}_3\text{PO}_4$ were 0.01793min⁻¹, 0.00102min⁻¹, 0.05301min⁻¹, 0.0229min⁻¹ and 0.0206min⁻¹, respectively. The maximum reaction rate constant

of 0.1 ZnCo₂O₄/Ag₃PO₄ is 0.05301min⁻¹, which is 3 times that of Ag₃PO₄ and 52 times that of ZnCo₂O₄. These results indicate that the combination of Ag₃PO₄ and ZnCo₂O₄ has a synergistic effect, which can improve its photocatalytic performance. Figure 5d shows the test of stability consequences of Ag₃PO₄ and 0.1ZnCo₂O₄/Ag₃PO₄ recycled three times. From the figure, it can be seen that after three rounds of recycling, the degradation rate of MO by Ag₃PO₄ is only 21.8%, while the degradation rate of Mo by 0.1 ZnCo₂O₄/Ag₃PO₄ is 84.4%, which indicates that the use of Ag₃PO₄ and ZnCo₂O₄ for compounding can improve the stability of the photocatalyst.

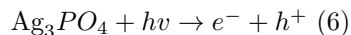
Figure6 Trapping experiments of active species during photocatalysis reaction.

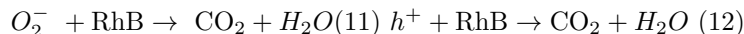
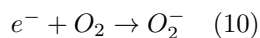
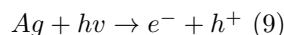
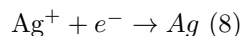
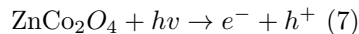
Fig. 6 shows the effect of different capture factors on the reaction rate of 0.1 ZnCo₂O₄/Ag₃PO₄ photocatalytic degradation of MO. From the figure, it can be seen that the addition of IPA has little influence on the photocatalytic degradation of MO. It can be seen that in the photocatalytic degradation of MO by 0.1 ZnCo₂O₄/Ag₃PO₄, holes (h⁺) and superoxide ions (O₂^{·-}) play the most important roles in the photocatalytic degradation, and hydroxyl radicals (OH[·]) play a partial role in the degradation.



Scheme 1 Schematic diagram of photocatalytic mechanism of ZnCo₂O₄/Ag₃PO₄.

Based on the aforesaid analysis, the reaction mechanism of the ZnCo₂O₄/Ag₃PO₄ photocatalytic degradation process was proposed. The valence band potential energy level of Ag₃PO₄ is about 2.9 eV, and the conduction band potential energy level is about 0.45 eV, so its band gap is 2.45 eV. The conduction band potential level of ZnCo₂O₄ is 0.145 eV, the valence band potential level is 2.775 eV, and its band gap width is 2.63 eV. Both ZnCo₂O₄ and Ag₃PO₄ can be excited by visible photons to form electron-hole pairs (Eq. (6-7)). With the accumulation of photogenerated electrons in the CB of Ag₃PO₄, Ag₃PO₄ was photoetched, which makes part of the Ag⁺ converted to singlet silver (Eq. (8)) [13]. Silver nanoparticles can absorb visible photons and form photoexcited electron hole pairs (Eq. (9)). [23]. Photogenerated electrons formed in Ag nanoparticles are captured by dissolved oxygen to form superoxide anions (O₂^{·-}) (Eq. (10)). The strong oxidation property of O₂^{·-} degrades MO to produce carbon dioxide and water (Eq. (11)). Meanwhile, the photogenerated electrons in the conduction band of ZnCo₂O₄ combine with the photogenerated holes generated by Ag nanoparticles to prevent further corrosion, making the catalyst itself self-stabilizing. The holes left in the valence bands of Ag₃PO₄ and ZnCo₂O₄ directly decomposed the MO oxidation to water and CO₂ (Eq. (12)). This is consistent with the active factor capture results.





4. Conclusion

In this paper, ZnCo_2O_4 was prepared by a microwave-assisted process, and then ZnCo_2O_4 was loaded onto Ag_3PO_4 by in-situ chemical precipitation method to obtain a composite photocatalyst. The catalytic activity and cycle stability were evaluated under visible light, and the catalytic reaction mechanism was proposed. The main conclusions are as follows:

(1) $\text{ZnCo}_2\text{O}_4/\text{Ag}_3\text{PO}_4$ exhibits high photocatalytic performance and good stability under room temperature and visible light conditions. The photocatalytic degradation rate of pure ZnCo_2O_4 within 30 minutes is only 5%, and the photocatalytic efficiency is very low. The results show that the degradation rate of MO by the 0.1 $\text{ZnCo}_2\text{O}_4/\text{Ag}_3\text{PO}_4$ composite system can reach 94% within 30 minutes, and MO is basically degraded. Research has found that ZnCo_2O_4 has a significant promoter effect on the photocatalytic degradation of Ag_3PO_4 .

(2) In the stability test, after three cycles, the degradation rate of MO by 0.1 $\text{ZnCo}_2\text{O}_4/\text{Ag}_3\text{PO}_4$ remained at 84.4%, while the degradation rate of Ag_3PO_4 was only 21.8%, indicating that the stability of the 0.1 $\text{ZnCo}_2\text{O}_4/\text{Ag}_3\text{PO}_4$ composite was significantly improved compared with Ag_3PO_4 . The photocatalytic activity was the highest at 0.1 $\text{ZnCo}_2\text{O}_4/\text{Ag}_3\text{PO}_4$. This study will play an important guiding role in pollution control.

(3) The visible light degradation of MO solution by Ag_3PO_4 is very easy to inactivate. The addition of ZnCo_2O_4 can accelerate the separation of photoelectron holes and improve the stability and catalytic activity of the catalyst.

References

- [1] Fujishima A. Photoelectrochemistry and photocatalysis will help us realize a green, sustainable future [J]. *Electrochemistry*, 2011, 79(10): 759.
- [2] Wu JM, Shih HC, Wu WT, Tseng YK, Chen IC. Thermal evaporation growth and the luminescence property of TiO_2 nanowires [J]. *J Cryst Growth*, 2005, 281(2): 384-390.
- [3] Mao J, Wu Q, Tao FF, Xu W, Hong TJ, Dong YL. Facile fabrication of porous BiVO_4 hollow spheres with improved visible-light photocatalytic properties [J]. *RSC Advances*, 2020, 10(11): 6395-6404.
- [4] Fagan R, McCormack DE, Dionysiou DD, Pillai SC. A review of solar and visible light active TiO_2 photocatalysis for treating bacteria, cyanotoxins and contaminants of emerging concern [J]. *Materials Science in Semiconductor Processing*, 2016, 42(1):2-14.
- [5] Cesaro A, Belgiorno V. Removal of endocrine disruptors from urban wastewater by advanced oxidation processes (AOPs): a review [J]. *The Open Biotechnology Journal*, 2016, 10(1):151-172.
- [6] Nakata K, Fujishima A. TiO_2 photocatalysis: Design and applications [J]. *Journal of photochemistry and photobiology C: Photochemistry Reviews*, 2012, 13(3): 169-189.
- [7] Marti E, Variatza E, Balcazar JL. The role of aquatic ecosystems as reservoirs of antibiotic resistance [J]. *Trends in microbiology*, 2014, 22(1): 36-41.
- [8] Fujishima A, Honda K. Electrochemical photolysis of water at a semiconductor electrode [J]. *nature*, 1972, 238(5358): 37-38.

- [9] Teng W, Li XY, Zhao QD, Chen GH. Fabrication of Ag/Ag₃PO₄/TiO₂ heterostructure photoelectrodes for efficient decomposition of 2-chlorophenol under visible light irradiation [J]. *Journal of Materials Chemistry A*, 2013, 1(32): 9060-9068.
- [10] Nosaka Y, Nosaka AY. Generation and detection of reactive oxygen species in photocatalysis [J]. *Chemical reviews*, 2017, 117(17): 11302-11336.
- [11] Li F, Zhang G, Song YH. Preparation and Photocatalytic Mechanism of Ag₃PO₄/SnO₂ Composite Photocatalyst [J]. *Nano*, 2019, 14(07): 1950092.
- [12] Li Y, Liu YF, Zhang MQ, Zhou QY, Li X, Chen TL, Wang SF. Preparation of Ag₃PO₄/TiO₂(B) heterojunction nanobelt with extended light response and enhanced photocatalytic performance [J]. *Molecules*, 2021, 26(22): 6987.
- [13] Liu DD, Zhu PY, Yin L, Zhang XY, Zhu KJ, Tan Jh, Jin RY. Facile fabrication of Bi₂GeO₅/Ag@Ag₃PO₄ for efficient photocatalytic RhB degradation [J]. *Journal of Solid State Chemistry*, 2021, 301: 122309.
- [14] Zheng CX, Yang H. Assembly of Ag₃PO₄ nanoparticles on rose flower-like Bi₂WO₆ hierarchical architectures for achieving high photocatalytic performance [J]. *Journal of Materials Science: Materials in Electronics*, 2018, 29:9291-9300.
- [15] Zhang XL, Wang N, Geng LL, Fu JN, Hu H, Zhang DS, Zhu BY, Carozza J, Han HX. Facile synthesis of ultrafine cobalt oxides embedded into N-doped carbon with superior activity in hydrogenation of 4-nitrophenol [J]. *Journal of Colloid and Interface Science*, 2012, 512: 844-852.
- [16] Che H, Liu A, Zhang X, Mu J, Bai Y, Hou J. Three-dimensional hierarchical ZnCo₂O₄ flower-like microspheres assembled from porous nanosheets: Hydrothermal synthesis and electrochemical properties [J]. *Ceramics International*, 2015, 41(6): 7556-7564.
- [17] Hung TF, Mohamed SG, Shen CC, Tsai YQ, Chang WS, Liu RS. Mesoporous ZnCo₂O₄ nanoflakes with bifunctional electrocatalytic activities toward efficiencies of rechargeable lithium-oxygen batteries in aprotic media [J]. *Nanoscale*, 2013, 5(24): 12115-12119.
- [18] Hung TF, Mohamed SG, Shen CC, Tsai YQ, Chang WS, Liu RS. Mesoporous ZnCo₂O₄ nanoflakes with bifunctional electrocatalytic activities toward efficiencies of rechargeable lithium-oxygen batteries in aprotic media [J]. *Nanoscale*, 2013, 5(24): 12115-12119.
- [19] Liu WH, Hu SQ, Wang Y, Zhang BB, Jin RY, Hu LS. Anchoring Plasmonic Ag@AgCl Nanocrystals onto ZnCo₂O₄ Microspheres with Enhanced Visible Photocatalytic Activity [J]. *Nanoscale Research Letters*, 2019, 14:1-10.
- [20] Schuhl Y, Baussart H, Delobel R, Bras ML, Leroy JM, Gengembre L, Grimblot J. Study of mixed-oxide catalysts containing bismuth, vanadium and antimony. Preparation, phase composition, spectroscopic characterization and catalytic oxidation of propene. *Journal of the Chemical Society Faraday Transactions 1*, 1983, 79: 2055-2069
- [21] Tan JH, Peng JH, Li Z, Liu DD, Li WB. Ag@AgBr/Ag₃PO₄ Nanocomposites as Photocatalyst for Degradation of Rhodamine B [J]. *Int. J. Electrochem. Sci*, 2021, 16(7).
- [22] Zhang X, Zhang L, Xie T, Wang D. Low-Temperature Synthesis and High Visible-Light-Induced Photocatalytic Activity of BiOI/TiO₂ Heterostructures. *Journal of Physical Chemistry C*, 2009, 113:7371-7378
- [23] Hu X, Ma Q, Wang X, Yang Y, Yang Y. Layered Ag/Ag₂O/BiPO₄/Bi₂WO₆ heterostructures by two-step method for enhanced photocatalysis. *Journal of Catalysis*, 2020, 387:28-38